In Vivo Confocal Scanning Laser Microscopy of Human Skin II: Advances in Instrumentation and Comparison With Histology[1]

Milind Rajadhyaksha,*† Salvador González,† James M. Zavislan,* R. Rox Anderson,† and Robert H. Webb†

*Lucid Inc., Henrietta, New York, U.S.A.; †Wellman Laboratories of Photomedicine, Department of Dermatology, Massachusetts General Hospital, Harvard Medical School, Boston, Massachusetts, U.S.A.

In 1995, we reported the construction of a video-rate scanning laser confocal microscope for imaging human skin *in vivo*. Since then, we have improved the resolution, contrast, depth of imaging, and field of view. Confocal images of human skin are shown with experimentally measured lateral resolution 0.5–1.0 μm and axial resolution (section thickness) 3–5 μm at near-infrared wavelengths of 830 nm and 1064 nm; this resolution compares well to that of histology which is based on typically 5 μm thin sections. Imaging is possible to maximum depth of 350 μm over field of view of 160–800 μm. A mechanical skin-contact device was developed to laterally stabilize the imaging site to within ± 25 μm in the presence of subject motion. Based on these results, we built a small, portable, and robust confocal microscope that is capable of imaging normal and abnormal skin morphology and dynamic processes *in vivo,* in both laboratory and clinical settings. We report advances in confocal microscope instrumentation and methods, an optimum range of parameters, improved images of normal human skin, and comparison of confocal images with histology.
Keywords: dermatology/morphology/non-invasive imaging/optical imaging. J Invest Dermatol 113:293–303, 1999

Confocal microscopy is a technique that allows optical sectioning of turbid objects (Wilson 1990; Pawley 1995; Webb, 1996). A thin plane or section can be optically or noninvasively imaged within a scattering medium with high resolution and contrast. We have shown that thin sections of human skin can be imaged *in vivo*, and nuclear and cellular detail can be visualized without biopsy and histologic processing (Rajadhyaksha *et al*, 1995).

Confocal microscopes (CM) provide a noninvasive window into living skin for basic and clinical research. Skin can be imaged in its native state either *in vivo* or freshly biopsied (*ex vivo*) without the fixing, sectioning, and staining that is necessary for routine histology. Dynamic processes can be noninvasively observed over an extended period of time. (The site being investigated can be marked with either tattoo ink particles or a marker ink pen. With a skin-contact device, the site can then be repeatedly located and imaged with reasonably good precision. This is further described in *Materials and Methods*.) Real-time near-infrared confocal microscopes may be potentially used in the clinic for imaging skin lesions and their margins prior to biopsy, diagnosis of lesions without biopsy, or detection of margins in freshly excised tumors. For example, we have characterized psoriasis *in vivo,* including microscopic margins that demarcate psoriatic plaques from the surrounding normal skin (Gonzalez *et al*, 1998).

Manuscript received August 28, 1998; revised May 19, 1999; accepted for publication May 25, 1999.

Correspondence: Dr. Milind Rajadhyaksha, MGH-Wellman Labs, Bartlett Hall Ext. 630, Boston, MA 02114, U.S.A. E-mail: rajadmil@helix.mgh.harvard.edu

Abbreviations: CM, confocal microscope; NA, numerical aperture.

[1]The authors have declared conflict of interest.

Imaging of human epidermis and superficial dermis *in vivo* has been demonstrated with white-light tandem scanning CM (New *et al*, 1991; Corcuff and Leveque, 1993; Corcuff *et al*, 1993, 1996; Bertrand and Corcuff, 1994; Kaufman *et al*, 1995) and with scanning laser CM (Rajadhyaksha *et al*, 1995; Masters *et al*, 1997). In 1995, we reported the design and development of a video-rate scanning laser CM (Rajadhyaksha *et al*, 1995). We imaged the epidermis and papillary dermis with moderate contrast, to a limited depth, and over a limited field of view, using visible and near-infrared wavelengths and a single oil immersion objective lens that provided fixed magnification, resolution, and working distance. A single detector aperture (pinhole) was used and the imaging rate was fixed at 30 frames per s (standard television rate in the U.S.A.). The mechanical fixture that interfaced the skin to the CM could be used only on forearms and the imaging site could not be efficiently stabilized. In subsequent research, we tested a range of parameters for improved resolution and contrast, deeper imaging, and wider fields of view with the use of longer near-infrared wavelengths, objective lenses with a range of magnifications and numerical aperture (NA) and longer working distances, a range of pinhole sizes, and variable imaging rates. A skin-contact device was developed that can precisely locate the field to be imaged and keep the skin laterally stable at different sites on the body. Confocal images were compared with the corresponding histology. Based on the experimental results, we developed a small and portable CM that can be easily moved between different labs and clinics. With this CM, we have imaged cellular and nuclear structure in the epidermis, collagen, and circulating blood cells in the dermis, and other structures such as sebaceous glands, hair, sweat ducts, and nails. In this study, we report advances in CM instrumentation and methods, an optimum range of parameters, improved images of normal human epidermis and dermis *in vivo*, and comparison of confocal images with histology.

MATERIALS AND METHODS

Subjects Sites on the arms, legs, back, torso, face, and scalp of human volunteers with skin types I–VI were imaged. Volunteers were recruited under experimental protocols that were approved by the Massachusetts General Hospital-Institutional Regulatory Board (MGH-IRB). Informed consent was obtained prior to confocal imaging.

Tested parameters The design and operation of our CM prototype has been previously reported (Rajadhyaksha *et al*, 1995). We tested the following range of parameters. Near-infrared illumination was as follows: 830 nm with a diode laser (SDL-2300-N2, Spectra Diode Laboratories, San Jose, CA; http://www.sdli.com), 1064 nm with an Nd:YAG laser (CV-4, Santa Fe Laser Company, Phoenix, AZ; this company has recently closed), and 1100 nm with a Ytterbium-doped fiber laser (prototype, Polaroid, Cambridge, MA; http://www.polaroid.com). The illumination power output from the objective lens (i.e., the power incident on the skin) was varied up to 20 mW. The illumination power was measured with a power meter (LM-3, Coherent, Auburn, CA; http://www.cohr.com), placed directly below the objective lens. The following water immersion objective lenses were tested for imaging the epidermis and dermis: 100×/1.2 NA, 50×/1.0 NA, 60×/0.85 NA, 30×/0.9–0.5 NA, 20×/0.75 NA, 40 ×/0.7 NA, and 40×/0.55 NA. Objective lens specifications are in appendix A. For imaging the stratum corneum, we used 63×/0.85 NA and 40×/0.65 NA dry (air immersion) objective lenses. Coverslips are used with those objective lenses that require one. Although the coverslips are fragile, we have found that they rarely break when imaging reasonably pliable skin sites, for two reasons: (i) when used with the skin-contact device (described below), the coverslip is only lightly pressed against the skin, and (ii) the objective lenses have sufficiently long working distances which prevents them from touching and pressing on the coverslip. On nonpliable sites such as the knuckles or knees, we do not use coverslips, and then correct for the resulting spherical aberration by varying the refractive index of the immersion medium (as explained below). Detector apertures (pinholes) of diameters 1–10 resels were used, where a resel is equal to one lateral resolution element. [A lateral resolution element is the minimum distance between two self-illuminated object points that can be distinctly seen as two separate points in the image (Webb, 1996).] The immersion media were water (refractive index n = 1.33) or cane-sugar solutions (of concentration 0%–57% in distilled water) of refractive indices n = 1.33–1.35. Although the objective lenses were designed to be used with water, we determined that spherical aberration in the CM optics could be reduced with immersion media of refractive indices slightly higher than that of water.[2] We have also used water-based gels, again, refractive indices n = 1.33–1.35, such as those used for ultrasound imaging (Aquasonic 100, Parker Laboratories, Fairfield, NJ; http://www.parkerlabs.com), ophthalmology (Goniosol, CIBA Vision, Atlanta, GA; http://www.cvo-us.com), surgical anti-bacterial lubricants (Surgilube, E. Fougera, Melville, NY; http://www.fougera.com), or commercial hair care (Vidal Sassoon Extra Hold Gel, Proctor & Gamble, Cincinatti, OH; http://www.pg.com). These viscous gels do not "run off" the skin as water does, especially when imaging awkwardly shaped sites such those as in **Fig B1** (*Appendix B*).

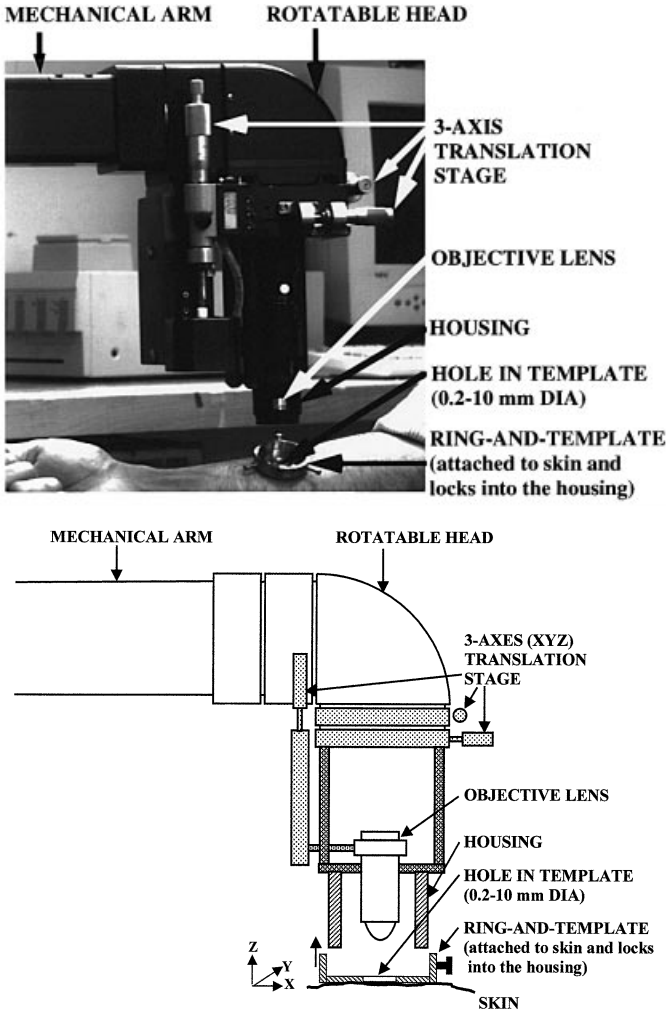

Figure 1. Skin-contact device keeps skin laterally stable to within ± 25 μm when imaging at different sites on the body. The skin-contact device consists of a housing for the objective lens, and a ring-and-template that is attached to the skin with medical-grade adhesive (either double-sided tape or liquid). The ring forms a well for holding the immersion medium. Holes in the template of diameter 0.2–10 mm allow precise location of the site to be imaged. By engaging and then locking the ring-and-template into the housing, we obtain stable skin-to-CM contact. The objective lens is mounted on a z-axis translation stage, so that the lens can be moved axially relative to the template. The housing is mounted on an XY-axes translation stage, so that the housing (and therefore the attached skin site) can be moved laterally relative to the objective lens.

CM instrumentation Based on the experimental test results, we built a small, portable and robust scanning laser CM (VivaScope, Lucid, Henrietta, NY; http://www.lucid-tech.com) with an optical design similar to that of the prototype (Figure 1 in Rajadhyaksha *et al*, 1995). The operating parameters are: illumination wavelength 830 nm, illumination power up to 20 mW on the skin, objective lens 30 ×/0.9 NA water immersion, field of view 250 μm, detector aperture (pinhole) diameters of 1–5 resels, and imaging rate 10–30 frames per s. The CM is supported on a stand that can be raised or lowered relative to the topographic site to be imaged; an extended arm with a rotatable head (**Fig 1**) allows easy interfacing to

[2]Spherical aberration causes loss of resolution and contrast in confocal images. Spherical aberration occurs due to CM optics and refractive index mismatch between the tissue and immersion medium. To determine the spherical aberration, we carried out interferometric tests on light-scattering gel-phantoms, as a model for the epidermis (Wan *et al*, 1999). The gel-phantoms were of refractive indices (n = 1.33–1.35) close to that (n = 1.34) of the epidermis. We found the spherical aberration to be mainly due to the spherical aberrations of the objective lens and coverslip not being completely balanced. This happens because of variations in coverslip thickness from their nominal (170 μm) thickness for which objective lenses are designed. Some objective lenses have correction collars to adjust for coverslip thickness variations; our objective lenses, however, do not have correction collars. Hence, we use the standard method of varying the refractive index of the immersion medium. The interferometric test showed that the spherical aberration could be reduced by using immersion media of refractive indices (n = 1.33–1.35) slightly different from the nominal refractive index (n = 1.33) for water. The interferometric test results are confirmed by the contrast of confocal images of human epidermis *in vivo*. When we use cane-sugar solutions of refractive indices n = 1.33–1.35, the visually perceived contrast in live images as well as the quantitatively measured contrast in grabbed images is higher than the contrast when using water (n = 1.33).

Note that we can get increased working distance by not using a coverslip, and then using a suitable immersion medium refractive index to correct for the resulting spherical aberration. For example, with the 100×/1.2 NA objective lens, the working distance increased from 150 μm to 320 μm by not using a coverslip. The interferometric measurements showed that the spherical aberration could be reduced to zero when using an immersion medium of refractive index 1.395. Again, this is confirmed with the contrast of confocal images of the epidermis *in vivo*. When we use cane-sugar solutions of refractive indices 1.39–1.40, the contrast is high in both visually perceived live images as well as grabbed images.

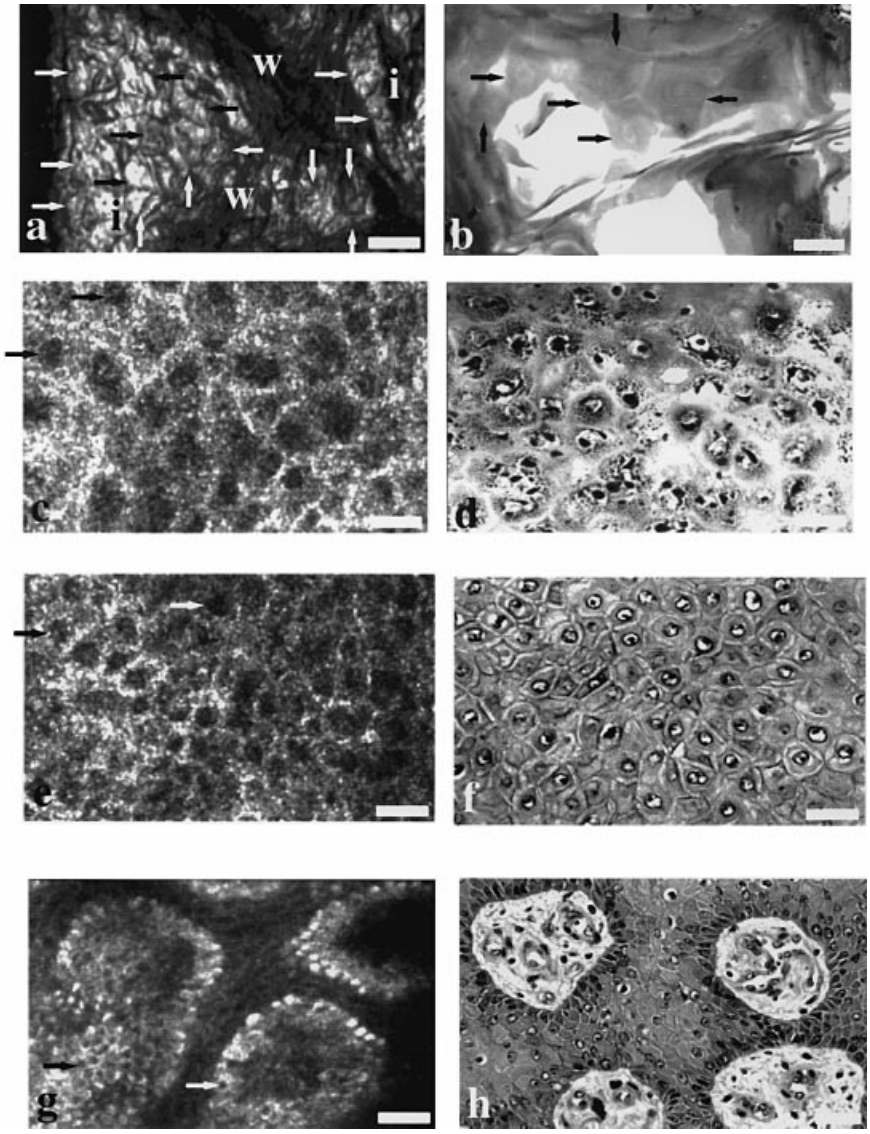

Figure 2. Water immersion objective lenses of NA 1.2–0.7 and detector aperture (pinhole) diameter of 1–5 resels improve resolution and contrast of human skin *in vivo*. Confocal images of horizontal (*en face*) sections in the epidermis (*a*, *c*, *e*, *g*) compare well to the corresponding histology (*b*, *d*, *f*, *h*). Both confocal images and histology sections of the epidermis show the following: (*a*, *b*) large, polygonal corneocytes (*arrows*) in the stratum corneum. The corneocytes are of size 10–30 μm in the confocal images and 30 μm in the histology. Nuclei are not seen within the corneocytes. In confocal images, the corneocytes (*a*, *arrows*) appear as bright polygonal shapes with dark outlines. The surface microtopography of the stratum corneum is seen as large "islands" (i) of corneocytes, separated by wrinkles (w) that appear as dark furrows; (*c*, *d*) granular cells of size 25–35 μm at average depths of 15–20 μm below the stratum corneum; (*e*, *f*) spinous cells of size 15–25 μm at average depths of 20–100 μm; (*g*, *h*) clusters of basal cells on dermal papillae at average depth of 100 μm. Basal cells are of size 7–12 μm. In confocal images of the viable epidermis, the bright areas are cytoplasm and the dark oval areas (*arrows* in *c*, *e*, *g*) within are the nuclei. Objective lenses and wavelengths: (*a*) 40×/0.65 NA dry, 830 nm; (*c*, *e*, *g*) 30×/0.9 NA water immersion, 830 nm; (*b*, *d*, *f*, *h*) 40×/0.65 NA dry, white light. *Scale bar*: 25 μm.

different sites on the arms, legs, back, torso, face, neck, and head (**Fig B1** in *Appendix B*).

Skin-contact device For stable imaging at different sites on the body, we developed a skin-to-CM contact device (**Fig 1**). The objective lens and the optical train after the galvanometric scanner were mounted on a mechanical arm, so that a subject can be easily placed either directly below or next to the objective lens (while lying on a gurney or sitting on a chair). The skin-contact device consists of a housing that encloses the objective lens, and a ring and template. The ring and template is attached to the skin with medical-grade adhesive, either double-sided tape (Vasamedics, St. Paul, MN; http://www.vasamedics.com) or liquid (Mastisol, Ferndale Labs, Ferndale, MI). The ring forms a well on the skin for holding the immersion medium. The template has a hole in the center to locate the site to be imaged. By using templates with hole diameters 0.2–10 mm, a site can be located to within that precision. With the subject placed either directly below or next to the objective lens, we lower or raise the CM on its stand as necessary, orient the head, and position the arm so that the ring-and-template engages and locks into the housing. The skin within the template hole then remains laterally stable relative to the objective lens even though the subject may be moving.

Imaging Details of the imaging procedure are in our earlier paper (Rajadhyaksha *et al*, 1995). The CM views horizontal *(en face)* sections within the skin instead of the vertical sections that are familiar from routine histology (**Fig 2** in Rajadhyaksha *et al*, 1995). While axially moving the objective lens relative to the skin with a three-axis translation stage, we imaged sections beginning at the stratum corneum and going through the epidermis and superficial dermis. In the confocal images, the different layers of the epidermis were identified by the depth of the imaged section, the appearance, and similarity to corresponding histology sections. Depth measurements were made relative to the stratum corneum, as explained previously (Rajadhyaksha *et al*, 1995). A sequence of confocal images were grabbed with an 8 bits/pixel frame grabber (Imaq PCI-1408 for PCs, National Instruments, Austin, TX, http://www.natinst.com; Pixelpipeline PTP425 for Macintosh computers, Perceptics Corporation, Knoxville, TN, http://www.perceptics.com; Scion AG-5 for PCs or Macs, Scion Corporation, Frederick, MD, http://www.scioncorp.com) and commercially available software (Imaqconf version 1.5.0 for PCs, National Instruments; SnagIt version 4.1 for PCs, TechSmith Corporation, East Lansing, MI, http://www.techsmith.com; IPLab Spectrum version 3.1 for Macs, Scanalytics, Fairfax, VA 22031, http://www.scanalytics.com; Scion version 1.6 for Macs or Scion ImagePC for PCs, Scion Corporation, Frederick, MD, http://www.scioncorp.com). Depending on the stability of the site, we were able to integrate two to four frames for improved signal-to-noise ratio. Four frames was the maximum number without introducing blurring due to skin motion. Each image requires about 1/3 MB and we have 100 MB of computer RAM available; thus, we could grab up to 300 frames over 10 s when imaging at 30 frames per s. The grabbed images were enhanced as follows: cropping, scaling with bilinear interpolation, linear 3×3 filtering (i.e., moving average of the matrix of 3×3 pixels using triangular shaped kernels), and contrast adjustment. The images were printed with a dye-sublimation printer (Phaser IISDX, Tektronix, Wilsonville, OR; http://www.tek.com).

Histology Punch skin biopsies (3 mm) were taken from the confocally imaged sites in three volunteers with skin types II, III, and IV, after local intradermal anesthesia (2% lidocaine with epinephrine). The sites were on

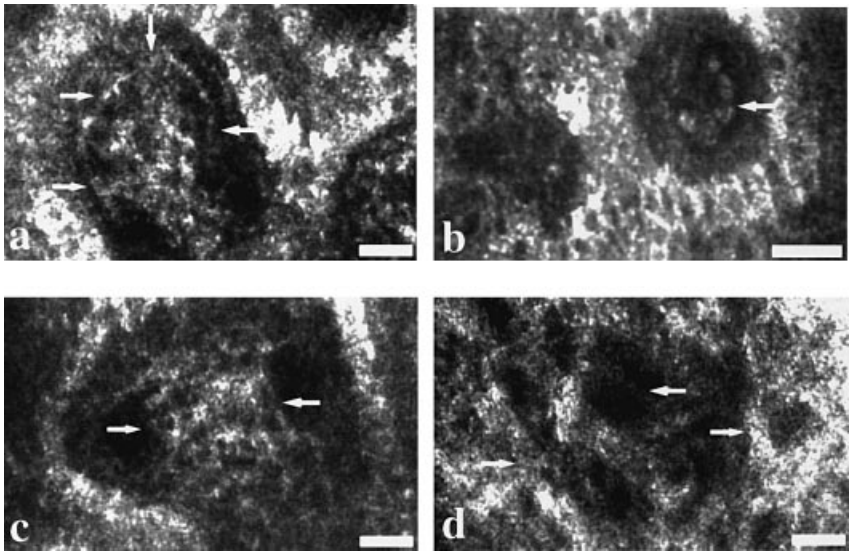

Figure 3. Longer near-infrared wavelengths increase depth of imaging in human skin *in vivo*. Confocal images of the dermis show: (*a*) blood flow (*arrows*) and (*b*) circulating blood cells (*arrows*) in the capillary loops which are, on average, 100–150 μm deep within dermal papillae; (*c*) papillary dermis and (*d*) superficial reticular dermis containing bundles (*arrows*) of diameter 5–25 μm at depth of 100–350 μm; these are probably collagen bundles. Objective lenses and wavelengths: (*a*, *c*, *d*) 30 ×/0.9 NA water immersion, 830 nm; (*b*) 100 ×/1.2 NA water immersion, 1064 nm. *Scale bar*: 25 μm.

the volar surface of their forearms. The skin biopsies were divided into two portions, fixed in buffered 10% formalin for 48 h, processed overnight, embedded in paraffin, sectioned at 5 μm thickness, and stained with hematoxylin and eosin. Standard vertical histology sections were made from one portion, and horizontal (*en face*) sections from the other. As the CM views horizontal sections, direct comparison of confocal images to horizontal histology sections was therefore possible. For one-to-one correspondence and to allow accurate visual comparison, both confocal images and histology micrographs were obtained with approximately the same lateral resolution (≈0.6 μm) over approximately the same field of view (≈200 μm). The horizontal histology sections of the different epidermal layers and the dermis were paired to the corresponding confocal images based on their appearance.

RESULTS

Improvements in resolution, contrast, depth of imaging, and field of view Table I lists the current optimum range of parameters and advances in the CM design with which we have improved confocal imaging of human skin *in vivo*. With objective lenses of NA 1.2–0.7, detector aperture diameter of 1 resel, and wavelength 1064 nm, the measured lateral resolution was 0.5–1 μm and axial resolution (section thickness) was 3–5 μm.[3] Further details of the resolution measurements are reported elsewhere (Rajadhyaksha *et al*, 1999). We determined that a pinhole diameter of 1 resel provides the highest axial resolution. When using objective lenses with high NA, however, we did not see a strong effect of pinhole diameter on image contrast. With the 30–100×/0.85–1.2 NA lenses, we have used pinholes of diameter up to 5 resels with only moderate decrease in contrast (i.e., the contrast was sufficiently high for the images to be useful). Deeper imaging was possible with longer near-infrared wavelengths: the maximum depth of imaging was 350 μm with either 1064 nm or 1100 nm when using the 30×/0.9 NA objective lens.[4] Objective lenses with widely varying magnification provided a widely varying field of view: 160–800 μm with 100–20× objective lenses. When using the skin-contact device, we observed on the live images that the site remained laterally stable to within ± 25 μm even though the subject was moving. There was a slow (≈1.25 Hz) axial modulation of the skin because of blood flow pulsation, but this did not affect the viewing or grabbing of images as our imaging at 10–30 frames per s was much faster.

Improved images of epidermis and dermis *in vivo* **Figure 2** shows confocal images of horizontal (*en face*) sections of the epidermis *in vivo* (**Fig 2*a***, ***c***, ***e***, ***g***) and comparative histology sections (**Fig 2*b***, ***d***, ***f***, ***h***). These confocal images were obtained with the small CM (VivaScope). A comparison of the images in this study (**Figs 2–5**) with earlier images (Figures 3–5 in Rajadhyaksha *et al*, 1995) shows the visual (qualitative) improvement in resolution and contrast.

The stratum corneum produces the first image of the top surface of the skin (**Fig 2*a***, ***b***) due to back-scattered light at the air–stratum corneum interface. Large, polygonal-shaped anucleated corneocytes are seen within the overall morphology of the stratum corneum. The corneocytes are 10–30 μm in the confocal images and 30 μm in the histology. [In this study, the size refers to the observed dimensions of the cells in the horizontal (*en face*) confocal sections; these dimensions directly relate to the cross-sectional area of the cells.] Nuclei are not seen within the corneocytes. The surface microtopography of the stratum corneum is seen as large "islands" of corneocytes, separated by wrinkles that appear as dark furrows. Within the islands, the corneocytes appear as bright polygonal shapes with dark outlines. At 15–20 μm below the stratum corneum, we see granular cells of 25–35 μm in size (**Fig 2*c***, ***d***). In confocal images of the viable cell layers of the epidermis, the cytoplasm appears bright and the nuclei are dark ovals. Within the cytoplasm, we see "grainy" structure due to organelles and melanosomes of

[3]Resolution measurements were made under a 150 μm thick layer of 10% Intralipid solution (Baxter Healthcare Corporation, Deerfield, IL; http://www.baxter.com) which is a standard light-scattering medium. The 10% intralipid solution approximately simulates scattering within skin as its scattering coefficients compare well to those of the epidermis at visible and near-infrared wavelengths. The lateral resolution was measured from the images of two standard objects: (i) the edge of a coverslip, and (ii) striae in the diatoms *Gyrosigma balticum*, *Surirella gemma*, *Navicula iyra*, and *Nitzschia sigma* (F6-B25D, Carolina Biological Supply Company, Burlington, NC; http://www.carolina.com), both immersed in 10% intralipid. The axial resolution (section thickness) was determined using the standard method of axially translating a mirror through the focus of the objective lens, and measuring the detected signal fall-off *versus* axial position. Again, the mirror was immersed in 10% intralipid. One measurement of axial resolution was determined with the mirror under a 80 μm thin piece of freshly excised living human epidermis that was removed as a suction-blister; this measurement accounts for scattering as well as spherical aberration in the epidermis.

[4]The maximum depth of imaging of 350 μm reported here is the measured distance along the axis that the objective lens was translated as we first imaged the stratum corneum, then through the epidermis, and into the dermis. Refractions of the focused illumination cone occur, however, due to the mismatch in refractive indices of the immersion medium (water, n = 1.33), stratum corneum (n = 1.51), epidermis (n = 1.34), and dermis (n = 1.40). These refractions cause an axial shift in the objective lens focal plane (i.e., confocal section). Geometrical analysis (see *Appendix C*) shows that the axial shift is 28 μm deeper when using the 30×/0.9 NA objective lens; thus, the maximum depth of imaging is estimated to be 378 μm.

Table I. Current optimum parameters and advances in CM design improve resolution, contrast, depth of imaging, and field of view of confocal images of human skin *in vivo*. For comparison, the initial parameters (Rajadhyaksha *et al*, 1995) are also listed

Parameters	Advances in 1998	Initial design (1995)
Illumination wavelengths	830, 1064, 1100 nm	488, 514, 647, 800 nm
Illumination power on the skin	up to 20 mW	up to 40 mW
Objective lens magnification and NA	100–20X/1.2–0.7 NA water immersion	100X/1.3 NA oil immersion
Detector aperture (pinhole) diameter	1–5 resels (resel = one lateral resolution element)	1 resel
Lateral resolution	0.5–1.0 μm (experimentally measured at 1064 nm)	0.3 μm (calculated at 800 nm)
Axial resolution (section thickness)	3–5 μm (experimentally measured at 1064 nm)	6 μm (experimentally measured at 800 nm)
Immersion medium refractive index	1.0 for top layers of stratum corneum 1.33–1.35 for subsurface layers of epidermis and dermis	1.52 (oil)
Maximum depth of imaging	350 μm (superficial reticular dermis) at 1064 nm	150 μm
Field-of-view	160–800 μm	160 μm
Working distance	0.15–2.0 mm	0.15 mm
Imaging rate	10–30 frames per s	30 frames per s
Mechanical features	Small, portable	Large, immobile
Skin-to-CM contact	Extended arm and rotatable head	Rigid fixture
Imaged sites on the body	Arms, legs, torso, back, face, scalp	Arms

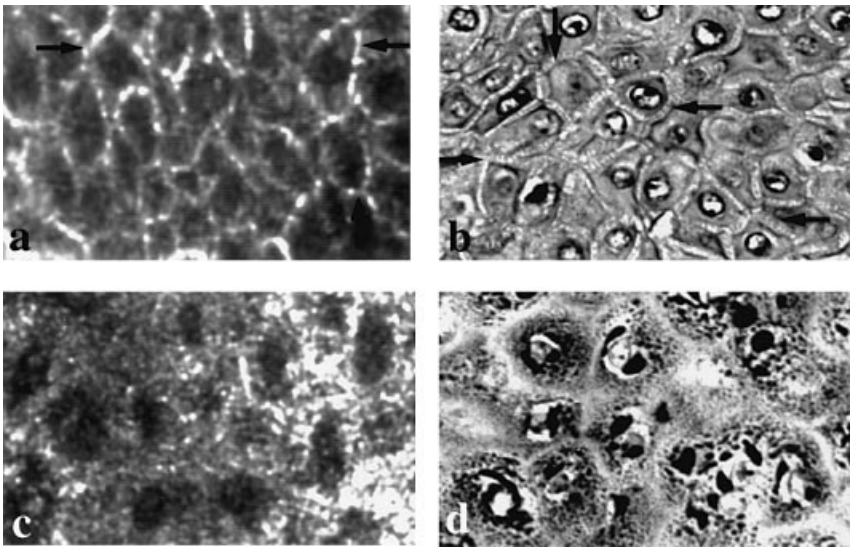

Figure 4. Bright punctate outlines of spinous cells in confocal images may be the desmosomes seen in histology. Both confocal images (*a*, *arrows*) and histology sections (*b*, *arrows*) showed that the cell outlines are more prominent in the spinous layers (*a*, *b*) than in the granular layers (*c*, *d*).

size on the order of the lateral resolution (0.5–1.0 μm). Spinous cells are smaller cells of size 15–25 μm (**Fig 2*e*, *f***), seen 20–100 μm below the stratum corneum. Below the spinous layers, at an average depth of 100 μm below the stratum corneum, we see a single layer of basal cells at the dermo–epidermal junction. Basal cells are 7–12 μm in size and are seen in clusters wherever the horizontal *(en face)* confocal section cuts across dermal papillae (**Fig 2 *g*, *h***).

Confocal images of horizontal (*en face*) sections of the dermis *in vivo* are shown in **Fig 3**. When we section below the dermo–epidermal junction, at average depths of 100–150 μm, we see blood flow in the capillary loops within each papilla (**Fig 3*a***); individual circulating blood cells are easily seen at higher resolution and magnification (**Fig 3*b***). From their relative shapes, sizes, and number densities, the cells were identified as erythrocytes of diameter 6–9 μm, leukocytes of dimension 6–30 μm, and platelets of dimension 2–5 μm. Below the dermo–epidermal junction, at average depths of 100–350 μm below the stratum corneum, a network of fibers of diameter 1–5 μm and bundles of diameter 5–25 μm can be seen within the papillary dermis (**Fig 3*c***) and superficial reticular dermis (**Fig 3*d***); these are probably collagen fibers and bundles.

Other structures that are visualized are faint spiral-shaped or crescent-shaped substructures that are either in the center or along the periphery within nuclei (presumed to be nucleoli), sebaceous glands, hair shafts within hair follicles, and sweat ducts spiralling into the dermis.

DISCUSSION

Working parameters

Use of the parameters in **Table I** has resulted in increased resolution and field of view, improved contrast, and deeper confocal imaging of human skin *in vivo*.

Illumination wavelength The longer near infrared 800–1100 nm wavelengths penetrate deeper than shorter visible 400–700 nm wavelengths that were used earlier (Anderson and Parrish, 1981). Both lateral resolution: $\Delta x = 0.46\ \lambda/NA$ and axial resolution (section thickness): $\Delta z = 1.4\ n\lambda/NA^2$ degrade linearly with wavelength λ (Sheppard and Wilson, 1978; Corle *et al*, 1986). The loss of resolution, however, was tolerable at 800–1100 nm. (The above equations define the theoretical resolution for a given refractive index n of the immersion medium. When imaging tissue which typically has local variations in refractive index, however, the actual resolution may be less due to spherical aberration from mismatch in the refractive indices of the immersion medium and tissue.)

Illumination power The illumination power was limited to 20 mW (measured) at the skin. Over a field of view of 160 × 120 μm with the 100×/1.2 NA objective lens, that results in an irradiance of 100 W per cm^2. This irradiance does not damage living human skin when imaged for several minutes. We imaged three sites on three volunteers of skin types II, III, and IV, for 15 min each with

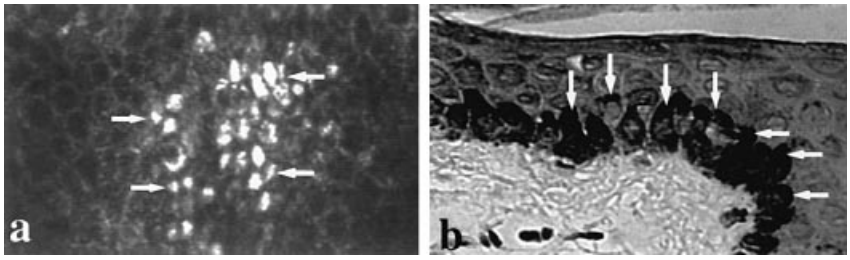

Figure 5. Confocal sections through the upper portions of basal cells show bright disks which may be the protective melanin "hats" located above the nuclei, that are seen in vertical sections of histology . The confocal image (*a*) and histology section (*b*, *arrows*) are from different subjects. The bright disks (*arrows*) are prominently seen in darkly pigmented skin (types IV–VI), and are always in supranuclear locations in only basal cells. These disks are not as bright in lightly pigmented skin (types I–III), and not seen in nonpigmented skin such as vitiligo.

the 100×/1.2 NA objective lens. The sites were then biopsied and processed for routine histology. Imaging was also done for 30 min on freshly excised (*ex vivo*) skin samples obtained from three volunteers, again, skin types II, III, and IV. The imaged samples were then processed for routine histology. In all cases, the histology did not show any damage to the skin samples.

The pigment melanin is the main chromophore (absorber of light) of visible and near-infrared light (Anderson and Parrish, 1981). Therefore, damage to pigmented skin and nevi (moles) is of concern. We recently completed a study to assess damage to pigmented tissue during confocal imaging.[5] The retinal pigmented epithelium contains a high concentration of melanin and therefore bovine retinal pigmented epithelium was used as a model for pigmented skin. Freshly biopsied living retinal pigmented epithelium samples were imaged for 5–20 min with irradiances of up to 950 W per cm^2 at the wavelength of 1100 nm. After the imaging, cell viability was quantitatively determined with a fluorescence microscope, using fluorescein diacetate to label living cells. Cell death was found to occur for irradiances exceeding 500 W per cm^2. The tissue damage was determined to be thermal. Note that we image with irradiances of 30–100 W per cm^2 depending on the objective lens (30–100×) and CM (prototype or VivaScope) used; this does not damage either nonpigmented or pigmented skin.

Objective lenses The use of water immersion objective lenses, instead of standard oil immersion, has the advantage that the refractive index of water (n = 1.33) is closer to that of the viable epidermis (n = 1.34) and dermis (n = 1.40) (Tearney *et al*, 1995). (By comparison, the refractive index of immersion oil is 1.52.) This minimizes spherical aberration and the consequent loss of resolution and intensity that occurs when imaging deep within living tissue (Sheppard and Cogswell, 1991; Sheppard and Gu, 1991).

The stratum corneum has a refractive index of 1.51 (Tearney *et al*, 1995) which does not match that of water. [Dehydrated stratum corneum has a slightly higher refractive index of about 1.55 (Scheuplein, 1964).] The stratum corneum is thin compared with the epidermis and dermis, however. Given that the spherical aberration due to a layer (that is placed in a converging or diverging beam) increases linearly with thickness but depends weakly on the refractive index (Bass *et al*, 1995), we expect the stratum corneum to have a weaker contribution to the aberration than the epidermis. Note that, when imaging through water with an oil immersion objective lens, the severe mismatch between the refractive index of immersion oil (n = 1.52, which is close to the n = 1.51 of the stratum corneum) and that of water (n = 1.33) produces spherical aberration at depths exceeding 5 μm below the oil–water interface (Carlsson, 1991; Gibson and Lanni, 1992; Hell *et al*, 1993).

Although water immersion objective lenses are necessary for imaging subsurface layers of living hydrated epidermis and dermis, the topmost layers of the stratum corneum can be better visualized by dry (air immersion) objective lenses. Contrast in confocal reflectance images is due to microvariations in refractive indices of tissue structures (Rajadhyaksha *et al*, 1995; Dunn *et al*, 1996, 1997), so that the higher refractive index mismatch between air (n = 1.00) and stratum corneum (n = 1.51) improves contrast and we can better visualize corneocytes and morphologic structure (compare **Fig 2*a*** in this study to Figure 3a in Rajadhyaksha *et al*, 1995). Note that the dry objective lenses can be used only for the topmost stratum corneum layers, and they do not image subsurface layers well.

Detector aperture (pinhole) diameter The size of the pinhole affects both axial resolution (section thickness) and detected signal level (Wilson and Carlini, 1987, 1988; Sandison *et al*, 1995). A small pinhole is necessary for high axial resolution (thin sections) but a large pinhole detects more light. We confirmed that a pinhole diameter of 1 resel provides the highest axial resolution or the thinnest sections. (This is the pinhole diameter defined in the plane of the skin. The actual pinhole diameter at the detector is the resel multiplied by the magnification of the objective lens and intermediate optics.) Although the section thickness increases with large pinholes, we did not see a strong effect of pinhole diameter on image contrast when using objective lenses with high NA. With the 30–100×/0.85–1.2 NA lenses, we have used pinholes of diameter up to 5 resels with only a moderate decrease in contrast (i.e., the contrast was sufficiently high for the images to be useful for easily visualizing nuclear and cellular detail in the epidermis and collagen and circulating blood in the dermis). Thus, with large pinholes, we lose some sectioning and contrast but, in return, we can either detect more signal or reduce illumination power on the skin.

Resolution With objective lenses of 1.2–0.7 NA, detector aperture diameter of 1 resel, and wavelength 1064 nm, the measured lateral resolution was 0.5–1 μm and axial resolution (section thickness) was 3–5 μm (Rajadhyaksha *et al*, 1999). The confocal section thickness *in vivo* is similar to the thickness (≈5 μm) of sections that are excised for histology; thus, the confocal resolution compares well with that of histology. As the confocal section thickness is less than the thickness (≈5–10 μm) of a single layer of cells, intracellular detail in the epidermis can be imaged.

When imaging the dermis (**Fig 3*c*, *d***), however, the resolution appears to degrade. This is probably due to the "hills-and-valleys" (dermal papillae-and-rete ridges) variation of the dermo–epidermal junction. The difference in refractive indices of the epidermis (n = 1.34) and the dermis (n = 1.40) must produce light scattering and spherical aberration effects at the highly irregular dermo–epidermal junction. Note that the resolution does not degrade when imaging, to comparable depth, tissues that lack irregular junctions between the different layers such as: (i) only the human dermis *in vivo* (overlying epidermis and dermo–epidermal junction removed as a suction-blister); (ii) human oral mucosa *in vivo*;[6] and (iii) rat bladder *in vivo* (Koenig *et al*, 1999).

[5]Lin D, Webb RH, Anderson RR, Rajadhyaksha M: Pigmented tissue damage with a confocal scanning laser microscope. *SPIE Biomedical Optics Symposium, Technical Abstracts Digest* 2–7, 1999 (abstr.)

[6]White WM, Rajadhyaksha M, Gonzalez SG, Fabian RL, Anderson RR: Clinical real-time confocal imaging of human oral mucosa *in vivo*. *J Invest Dermatol* 110:588, 1998 (abstr.)

Skin-to-CM contact Observation of live images shows that the imaged site remains laterally stable to within ± 25 μm (about ± 2 cells) even though the subject was moving. We observed the lateral shifts of ± 25 μm to occur over 15–60 s (150–1800 frames at 10–30 frames per s), depending on the subject and the skin site. Because these lateral shifts in the image occur very slowly compared with the much faster imaging rates of 10–30 frames per s, they do not degrade the lateral resolution of 0.5–1.0 μm or blur the image.

The diameter of the ring-and-template is 3 cm which defines the available contact area for attaching it to the skin. The large contact area allows the ring-and-template to be easily attached on sites where the skin is either inherently flat or easily deforms into a flat surface. It is, however, not necessary to use the entire available contact area. The template is thin and can slightly deform to fit curved surfaces; thus, we have been able to attach the ring-and-template with minimal contact area to several different nondeformable curved sites on the body (**Fig B1** in *Appendix B*).

We can mark the site being studied with tattoo ink particles of ≈50–100 μm in diameter that are injected along the periphery of the hole in the template. The tattoo ink particles last for several months. Alternatively, we can mark the periphery of the hole with a marker ink pen. The marker ink lasts for only 2–3 d, so that the site has to be re-marked often. Once the site has been marked, we have been able to remove the ring-and-template, and subsequently attach it at the same site with reasonably good precision. Thus, a specific site can be repeatedly located and imaged multiple times over several months.

A limitation of using the ring-and-template is that only the skin within the hole can be imaged. For imaging either the skin that lies immediately beyond the hole or multiple sites that are close to each other, the ring-and-template has to be removed and re-attached. This may result in the loss of a few layers of stratum corneum from under the template. This can be minimized, however, with the use of a larger ring-and-template (with a larger hole) and larger objective lens housing.

Image prints The images presented in this study were printed with a dye-sublimation printer. Although a dye-sublimation printer produces photographic-quality prints, we have found that the latest inexpensive ink-jet printers (e.g., HP 720C, Hewlett-Packard, Palo Alto, CA; http://www.hp.com) or laser printers (e.g., HP 4000, Hewlett-Packard) can also produce reasonably good quality prints.

Confocal images *versus* histology

The stratum corneum in the confocal images (**Fig 2*a***) appears different from that (**Fig 2*b***) in the histology. Imaging with a dry objective lens enhances the surface microtopography of the stratum corneum which appears as islands of corneocytes separated by wrinkles. The corneocytes appear as bright polygonal shapes with dark outlines. In histology, the stratum corneum appears different due to the artifact of lateral and vertical stretching; consequently, the corneocytes are larger than those seen in the confocal images. In the granular, spinous, and basal cell layers (**Fig 2*c–h***), however, there is good visual (qualitative) similarity of the confocal images to histology. Quantitative analysis of cellular and morphologic features showed good correlation of confocal images to those in histology (Figures 7 and 8 in Rajadhyaksha *et al*, 1995). Features that were analyzed were cell and nuclear size, nuclear/cytoplasm ratio, cellular (or nuclear) density, density and size of dermal papillae, thickness of stratum corneum, epidermis, and rete ridges, blood cell type (platelets *versus* erythrocytes *versus* leukocytes) and size, and blood vessel size.

Confocal images are completely noninvasive and therefore free of the artifacts of the tissue processing (biopsy, fixing, sectioning, staining) that is necessary for histology. In the confocal images (**Fig 2*a***, ***c***, ***e***, ***g***), we see grainy structure within the cytoplasm due to organelles and melanosomes of size on the order of the lateral resolution of 0.5–1.0 μm; when the corresponding histology (**Fig 2*b***, ***d***, ***f***, ***h***) is viewed with the same resolution, this grainy structure is seen in the granular layers but is not apparent in the spinous and basal layers. Artifacts in confocal images are (i) bright or dark spherical disks on the skin surface due to bubbles or dirt in the immersion medium, and (ii) bright dots in the center of nuclei which occasionally occur due to back-reflection of the illuminating cone of light from the underlying spherically shaped nuclear membrane. Artifacts in histology are shrinkage (causing empty spaces), distortion during biopsy, folds or wrinkles, precipitate particles, and dissolution of lipids; all these lead to disruption of the stratum corneum and corneocytes, and degeneration of cells and morphology including shrinkage of nucleoli (Ham and Cormack, 1979). Confocal microscopy can noninvasively image dynamic changes such as, for example, blood flow, effects of ultraviolet light exposure,[7] response to allergens (Gonzalez *et al*, 1999a), response to laser treatment (Gonzalez *et al*, 1999b), and inflammation (Gonzalez *et al*, 1999c). By comparison, the biopsy for histology destroys the site being investigated such that information at only one time point can be obtained.

The granular cells and spinous cells may appear similar to each other in the two confocal images (**Fig 2*c***, ***e***) shown here; however, the morphology changes as we go deeper into the epidermis. The morphologic changes may not be apparent when seen in only two images, but are obvious when seen in either real-time or a grabbed sequence of several images. From the superficial to the deeper spinous layers, there is a decrease in cell and nuclear size and an increase in the nuclear/cytoplasm ratio, cell density, and melanin content. We have quantitatively and qualitatively analyzed these morphologic changes and shown good correlation to histology; the data have been previously reported (Rajadhyaksha *et al*, 1995).

Often, cells appear to have bright punctate outlines when seen under high resolution with the 100×/1.2 NA objective lens (**Fig 4*a***). These appear more prominently in the spinous layers (**Fig 4*a***) than in the granular layers (**Fig 4*c***), similar to that seen in histology (**Figs 4*b***, ***d***). These bright cell outlines may be desmosomes. Desmosomes are known to be punctate spine-like cytoplasmic processes (containing thin filaments) that extend between cells to provide intercellular adhesion (Ham and Cormack, 1979; Fawcett, 1986; Goldsmith 1991); thus, the cell outlines appear punctate in the confocal images. They appear bright probably because the cytoplasmic processes back-scatter light, similar to that from intracellular cytoplasm. [As noted earlier, the contrast in confocal reflectance images is due to refractive index variations in the tissue microstructures; thus, the cytoplasm scatters back light and appears bright (Rajadhyaksha *et al*, 1995; Dunn *et al*, 1996, 1997)]. The bright cell outlines are not seen in the stratum corneum probably because: (i) the desmosomes may have degenerated (Fawcett, 1986; Goldsmith 1991), or (ii) the confocal section thickness of 3–5 μm includes several closely stacked layers of tightly packed corneocytes such that the desmosomes between cells may not be detected (i.e., may not image with high contrast) within the highly keratinized, strongly back-scattering bright cytoplasm.

In basal cells, confocal sections through the upper portion of the cells show bright disks (**Fig 5*a***). The disks always occur in supranuclear positions and are prominent in darkly pigmented skin (types IV–VI). We know that melanin provides strong contrast and appears bright in confocal images, such that the epidermal keratinocytes in darkly pigmented skin images brighter than those in lightly pigmented skin (Rajadhyaksha *et al*, 1995). Thus, the brightness and supranuclear location of these disks suggests that these may be the protective melanin "hats" located above the nuclei, that are seen in high resolution histology (**Fig 4*b***; see also Stenn, 1988). These disks are not as bright in lightly pigmented skin (types I–III), and not seen in nonpigmented skin such as vitiligo.

[7]Ugent SJ, Rajadhyaksha M, Kollias N, Anderson RR: *In vivo* scanning laser confocal microscopy of UVB-irradiated human skin. *Photochem Photobiol* 63:50s, 1996 (abstr.)

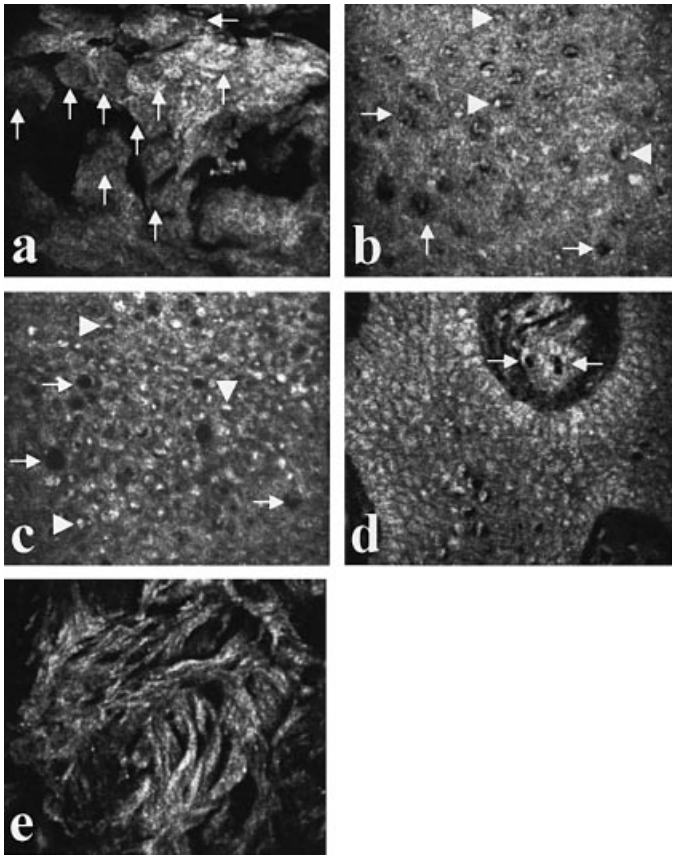

Figure 6. The gross architecture of the epidermis and dermis in confocal images of horizontal (*en face*) hematoxylin and eosin-stained sections appears similar to that seen *in vivo* (Fig 2). The confocal images of the histology sections show (*a*) large polygonal corneocytes (*arrows*) without nuclei, (*b*) granular, (*c*) spinous, and (*d*) basal cell layers. The cytoplasm is bright and grainy, and the nuclei appear as dark ovals (*b*,*c*, *arrows*). Within the dark nuclei, nucleoli are clearly seen as bright oval structures (*b*,*c*, *arrowheads*). Although not evident in this figure, the intercellular outlines are dark. Blood vessels are clearly seen in cross-section (*d*, *arrows*) within dermal papillae. Collagen bundles in the dermis (*e*) can be imaged with high resolution and contrast.

Confocal images in vivo versus *confocal images of hematoxylin and eosin-stained skin* When fixed and hematoxylin and eosin-stained horizontal (*en face*) histology sections are viewed with the CM (**Fig 6**), the gross architecture of the skin appears similar to that seen in the confocal images *in vivo* (**Fig 2**). Specific features are better delineated in the histology sections than *in vivo*, however, due to the enhanced contrast from the hematoxylin and eosin stains. Thus, **Fig 6** provides additional insight into the interpretation of confocal reflectance images of human skin that are obtained with scanning CM under coherent laser illumination. (Note, however, that hematoxylin and eosin-stained histology sections are normally viewed with a conventional microscope using incoherent white-light illumination. As the histology sections are typically 5 μm thin, the optical sectioning capability of a confocal microscope is not necessary for viewing these sections.)

Within the stratum corneum, large polygonal anucleated corneocytes are seen (**Fig 6*a***), similar to those seen *in vivo* (**Fig 2*a***). The dark outlines of the corneocytes and the surface microtopography that are prominent *in vivo* are, however, not seen in the hematoxylin and eosin-stained sections. This must be due to the histologic processing. As expected, in the granular, spinous, and basal cell layers, the cytoplasm appears bright and grainy, and the nuclei appear as dark ovals (**Fig 6*b–d***); this is also seen *in vivo* (**Fig 2*c***, ***e***, ***g***). The grainy appearance of cytoplasm under coherent laser illumination shows, to some extent, the effect of speckle produced by diffusely back-scattered light from the optically rough tissue microstructure. [Optically rough means that the size variations of the microstructures are on the order of the illumination wavelength. This, then, causes spatial variations in the phase of the detected wavefront which produces speckle across the detector aperture (Goodman, 1985).] By comparison, the cytoplasm appears much less grainy when illuminated with incoherent white light in both human skin *in vivo* (imaged with tandem scanning CM) and stained hematoxylin and eosin sections (viewed with a conventional microscope). Confocal images of the hematoxylin and eosin-stained sections shows the nucleoli as bright oval structures inside nuclei (**Fig 6*b***, ***c***). Correspondingly, confocal images of skin *in vivo* show faint spiral-shaped or crescent-shaped structures inside the nuclei, which we think may be the nucleoli. The nucleoli that are seen so well in the hematoxylin and eosin-stained sections are not easily seen *in vivo*, probably because they back-scatter weakly and lack image contrast.

As noted earlier, in the epidermis *in vivo*, we observe bright punctate cell outlines which were more prominent in the spinous layers than in the granular layers (**Fig 4*a***, ***c***). This compares well with the histology (**Fig 4*b***, ***d***). These bright outlines may be desmosomes. The bright outlines of spinous cells that are seen *in vivo* (**Fig 4*a***) are not seen in the corresponding confocal images of hematoxylin and eosin-stained sections (**Fig 6*c***). Although not evident in **Fig 6**(***c***), the spinous cell outlines consistently appear dark in the live images. This suggests that the back-scattered light from the desmosomes may be much less in the hematoxylin and eosin-stained sections than that *in vivo*. This must be because the desmosomes appear to be few in number and spaced far apart compared with the CM illumination spot diameter (when the sections are viewed with a conventional microscope). This suggests degradation of the desmosomes during histologic processing. Electron microscopy supports this finding; electron micrographs reveal few desmosomes and large air gaps between cells, indicating loss of intercellular structure (Goldsmith 1991).

Collagen bundles in the hematoxylin and eosin-stained sections (**Fig 6*e***) appear bright and can be visualized with high resolution, compared with the relatively less bright structures *in vivo* that are imaged with lower resolution and contrast (**Fig 3*c***, ***d***). This is probably due to the effects of the overlying epidermis, as noted earlier; when the epidermis is removed (as a suction blister), the confocal images of collagen in the dermis *in vivo* compare very well with **Fig 6**(***e***). The blood vessels and dynamic blood flow in the dermis that is easily imaged *in vivo* (**Fig 3*a***, ***b***) is not seen in the hematoxylin and eosin-stained sections. In these sections, however, the cross-sections of the blood vessels containing blood cells are clearly delineated within dermal papillae (**Fig 6*d***).

CONCLUSIONS

We have determined an optimum range of parameters for CM that improves resolution and contrast, and increases the field of view and maximum depth of imaging in human skin *in vivo*. A small, portable, and robust CM was developed for rapid set-up and easy use in laboratory and clinical settings. Real-time noninvasive confocal infrared imaging of the epidermis, papillary dermis, and superficial reticular dermis to a maximum depth of 350 μm is possible with good correlation to histology.

Further instrumentation development will be toward vertical sectioning, three-dimensional image reconstruction, increasing the field of view, improving skin-to-microscope contact, and smaller (possibly hand-held) size. The scientific challenges are to learn to interpret and analyze confocal images, and improve confocal images-to-histology correlation. Real-time confocal microscopy will be potentially useful for basic and clinical research, and for screening and diagnosis of lesions without biopsy.

Development of the CM prototype was funded in parts by DOE grant DE-FG02–91ER61229 and by a grant from the Whitaker Foundation to Milind

Rajadhyaksha. Development of the small and portable CM was partly funded by SBIR grant 1R43CA580540 from the National Cancer Institute-NIH to Lucid. Human studies were supported by Lucid.

REFERENCES

Anderson RR, Parrish JA: The optics of human skin. *J Invest Dermatol* 77:13–19, 1981

Bass M, Van Stryland EW, Williams DR, Wolfe WL (eds): *Handbook of Optics*, Vol. II. New York: McGraw-Hill, 1995, p 7.5

Bertrand C, Corcuff P: In vivo spatio-temporal visualization of the human skin by real-time confocal microscopy. *Scanning* 16:150–154, 1994

Carlsson K: The influence of specimen refractive index, detector signal integration, and non-uniform scan speed on the imaging properties in confocal microscopy. *J Microsc* 163:167–178, 1991

Corcuff P, Leveque JL: In vivo vision of the human skin with the tandem scanning microscope. *Dermatology* 186:50–54, 1993

Corcuff P, Bertrand C, Leveque JL: Morphometry of human epidermis in vivo by real-time confocal microscopy. *Arch Dermatol Res* 285:475–481, 1993

Corcuff P, Gonnord G, Pierard GE, Leveque JL: In vivo confocal microscopy of human skin: a new design for cosmetology and dermatology. *Scanning* 18:351–355, 1996

Corle TR, Chou CH, Kino GS: Depth response of confocal optical microscopes. *Opt Lett* 11:770–772, 1986

Dunn AK, Smithpeter C, Welch AJ, Richards-Kortum R: Sources of contrast in confocal reflectance imaging. *Appl Opt* 35:3441–3446, 1996

Dunn AK, Smithpeter C, Welch AJ, Richards-Kortum R: Finite-difference time-domain simulation of light scattering from single cells. *J Biomed Opt* 2:262–266, 1997

Fawcett DW: *A Textbook of Histology*, 11th edn. Philadelphia: W.B. Saunders, 1986, pp 69, 550

Gibson SF, Lanni F: Experimental test of an analytical model of aberration in an oil-immersion objective lens used in three-dimensional light microscopy. *J Opt Soc Am A* 9:154–166, 1992

Goldsmith LA (ed.): *Physiology, Biochemistry, and Molecular Biology of the Skin*, 2nd edn. New York: Oxford University Press, 1991, pp. 5–6, 11, 18.

Gonzalez S, Rajadhyaksha M, Anderson RR: Non-invasive (real-time) imaging of histologic margins of a proliferative skin lesion *in vivo*. *J Invest Dermatol* 111:538–539, 1998

Gonzalez S, Gonzalez E, White WM, Rajadhyaksha M, Anderson RR: Allergic contact dermatitis: correlation of *in vivo* confocal imaging to routine histology. *J Am Acad Dermatol* 40:708–713, 1999a

Gonzalez S, White WM, Rajadhyaksha M, Anderson RR, Gonzalez E: Confocal imaging of sebaceous gland hyperplasia in vivo to assess efficacy of pulsed dye laser treatment. *Lasers Surg Med* in press, 1999b

Gonzalez S, Rajadhyaksha M, Gonzalez-Serva A, White WM, Anderson RR: Confocal reflectance imaging of folliculitis *in vivo:* correlation with routine histology. *J Cutan Pathol* 26:201–205, 1999c

Goodman JW: *Statistical Optics*. New York: John Wiley & Sons, 1985, pp 347–356

Ham AW, Cormack DH: *Histology*, 8th edn. Philadelphia: J.B. Lippincott, 1979, pp 22–24, 618–619

Hell S, Reiner G, Cremer C, Stelzer EHK: Aberrations in confocal fluorescence microscopy induced by mismatches in refractive index. *J Microsc* 169:391–405, 1993

Kaufman SC, Beuerman RW, Greer DL: Confocal microscopy: a new tool for the study of the nail unit. *J Am Acad Dermatol* 32:668–670, 1995

Koenig F, Gonzalez S, White WM, Lein M, Rajadhyaksha M: Near-infrared confocal laser scanning microscopy of bladder tissue in vivo. *Urology* 53:853–857, 1999

Masters BR, Aziz DJ, Gmitro AF, Kerr JH, O'Grady TC, Goldman L: Rapid observation of unfixed, unstained human skin biopsy specimens with confocal microscopy and visualization. *J Biomed Opt* 2:437–445, 1997

New KC, Petroll WM, Boyde A, *et al*: In vivo imaging of human teeth and skin using real-time confocal microscopy. *Scanning* 13:369–372, 1991

Pawley JB (ed.): *Handbook of Biological Confocal Microscopy*, 2nd edn. New York: Plenum Press, 1995

Rajadhyaksha M, Grossman M, Esterowitz D, Webb RH, Anderson RR: *In vivo* confocal scanning laser microscopy of human skin: melanin provides strong contrast. *J Invest Dermatol* 104:946–952, 1995

Rajadhyaksha M, Anderson RR, Webb RH: Video-rate confocal scanning laser microscope for imaging human tissues *in vivo*. *Appl Opt* 38:2105–2115, 1999

Sandison DR, Piston DW, Williams RM, Webb WW: Quantitative comparison of background rejection, signal-to-noise ratio, and resolution in confocal and full-field scanning microscopes. *Appl Opt* 34:3576–3588, 1995

Scheuplein RJ: A survey of some fundamental aspects of the absorption and reflection of light by tissue. *J Soc Cosmet Chem* 15:111–122, 1964

Sheppard CJR, Cogswell CJ: Effects of aberrating layers and tube length on confocal imaging properties. *Optik* 87:34–38, 1991

Sheppard CJR, Gu M: Aberration compensation in confocal microscopy. *Appl Opt* 30:3563–3568, 1991

Sheppard CJR, Wilson T: Depth of field in the scanning microscope. *Opt Lett* 3:115–117, 1978

Stenn KS. The skin. In: Weiss L (eds). *Cell and Tissue Biology*. Baltimore: Urban and Schwarzenberg, 1988, p 548

Tearney GJ, Brezinski ME, Southern JF, Bouma BE, Hee MR, Fujimoto JG: Determination of the refractive index of highly scattering human tissue by optical coherence tomography. *Opt Lett* 20:2258–2260, 1995

Visser TD, Oud JL, Brakenhoff GJ: Refractive index and axial distance measurements in 3-D microscopy. *Optik* 90:17–19, 1992

Wan DS, Rajadhyaksha M, Webb RH: Elimination of spherical aberration in confocal images of specimens with refractive indices 1.33–1.40. *J Microscopy*, in press, 1999

Webb RH: Confocal optical microscopy. *Rep Prog Phys* 59:427–471, 1996

Wilson T (ed.): *Confocal Microscopy*. San Diego: Academic Press, 1990

Wilson T, Carlini AR: Size of the detector in confocal imaging systems. *Opt Lett* 12:227–229, 1987

Wilson T, Carlini AR: Three-dimensional imaging in confocal imaging systems with finite sized detectors. *J Microsc* 149:51–66, 1988

APPENDIX A

Table AI. Water immersion and dry (air immersion) objective lenses used for imaging the stratum corneum, epidermis, and dermis[a]

Objective lens and coverslip requirement	Product number and manufacturer	Degree of correction	Working distance
100×/1.2 NA, water, with coverslip	518039, Leica	Planachromat	0.15 mm
50×/1.0 NA, water, with coverslip	518043, Leica	Planachromat	0.12 mm
60×/0.85 NA, water, without coverslip	1UM571, Olympus	Planachromat	2.0 mm
30×/0.9-0.5 NA, water, with coverslip and adjustable iris	96008 LOMO, Vermont Optechs	Planachromat	1.5 mm
20×/0.75 NA, multi-immersion, infinity corrected, with correction collar, and with or without coverslip	93146, Nikon	Planachromat	0.35 mm
40×/0.7 NA, water, without coverslip	1-LB450, Olympus	Planachromat	3.1 mm
40×/0.55 NA, water, without coverslip	85063, Nikon	Achromat	3.9 mm
63×/0.85 NA, dry, without coverslip	04OAS018, Melles Griot	Achromat	0.14 mm
40×/0.65 NA, dry, without coverslip	04OAS016, Melles Griot	Achromat	0.42 mm

[a]These lenses are from Leica (Malvern, PA; http://www.leica.com), Olympus (Lake Success, NY; http://www.olympus.com), Vermont Optechs (Charlotte, VT; http://www.scopeshop.com), Nikon (Melville, NY; http://www.nikon.com), and Melles Griot (Irvine, CA; http://www.mellesgriot.com). All objective lenses are corrected for tube length of 160 mm, and without any correction collars or adjustable irizes, except where noted. The immersion media are either water (refractive index 1.33) or air (refractive index 1.0). One objective lens (20 ×/0.75 NA, 93146, Nikon) is multi-immersion with the immersion media being water, glycerine, or oil (refractive indices 1.33, 1.47, and 1.52, respectively); we used this lens with water only.

APPENDIX B

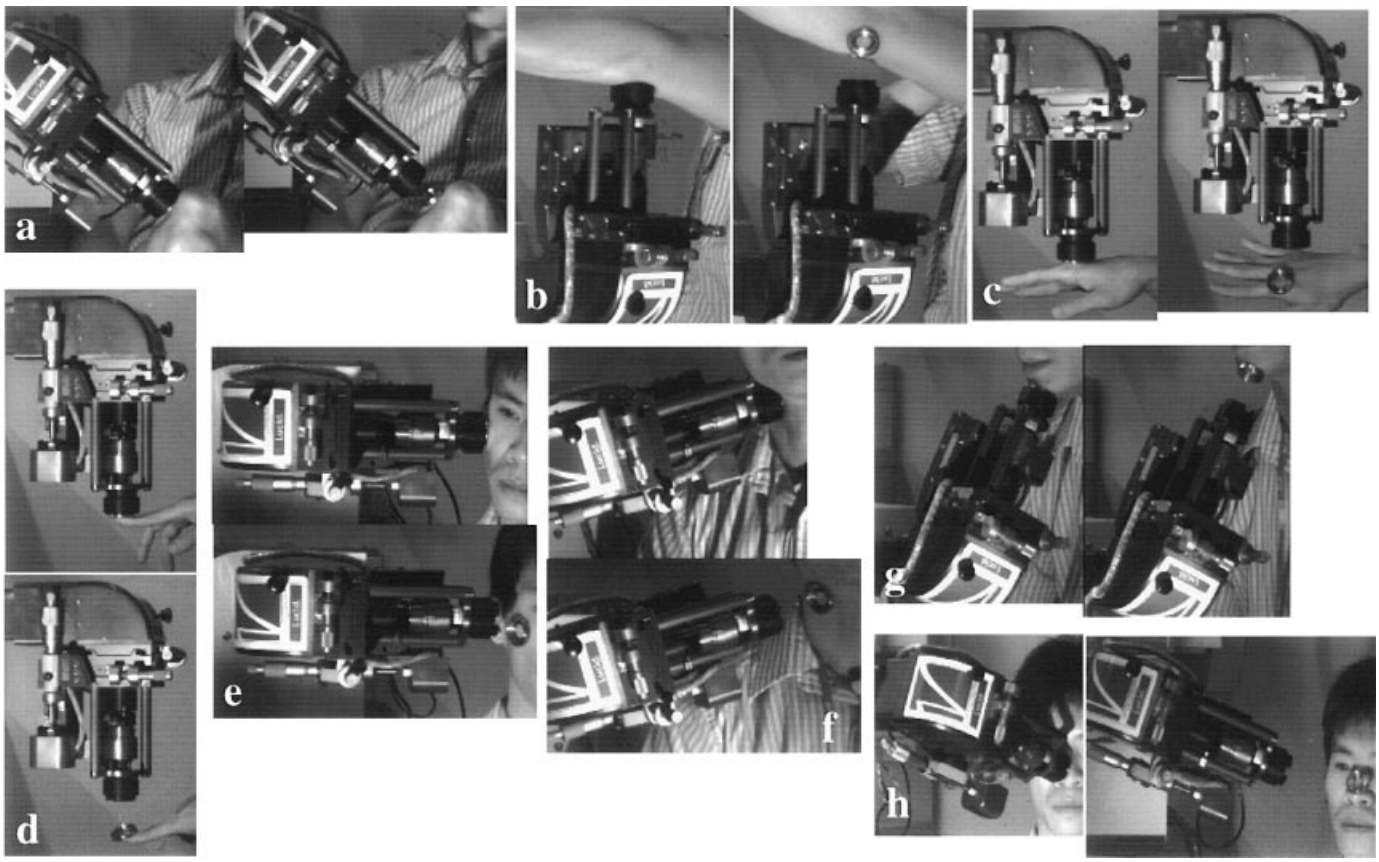

Figure B1. The skin-contact device can be used on either flat, deformable, or non-deformable curved skin surfaces. The ring-and-template can be attached with minimal contact area to sites on the knees (*a*), elbows (*b*), knuckles (*c*), nails (*d*), cheeks (*e*), neck (*f*), chin (*g*), and nose (*h*).

APPENDIX C

In this appendix, we analyze the axial shift in the objective lens focal plane (i.e., confocal section) due to the mismatch in the refractive indices of the immersion medium (water), stratum corneum, epidermis, and dermis (see also Visser *et al*, 1992; Carlsson, 1991). Refraction at the interface between two media causes a light ray to bend (**Fig C1**) such that the actual depth below the interface is

$$y_2 = y_1 \frac{\tan\theta_1}{\tan\theta_2} \quad \text{(C.1)}$$

where y_1 is the apparent or nominal depth (in the absence of refraction), n_1 and n_2 are the refractive indices of the two media and θ_1 and θ_2 are the angles of incidence and refraction, respectively. Snell's law relates θ_2 to θ_1:

$$n_2 \sin\theta_2 = n_1 \sin\theta_1. \quad \text{(C.2)}$$

We model the immersion medium and the three layers (stratum corneum, epidermis, dermis) of human skin as plane parallel layers with uniform refractive indices (**Fig C2**). The following analysis determines the axial shift in the objective lens focal plane (i.e., cofocal section) based on geometrical optics analysis of the marginal rays of the cone of light that is focused by the objective lens.

There are three interfaces (**Fig C2**) across which the refractive index changes: between the immersion medium and stratum corneum (I–SC), the stratum corneum and epidermis (SC–E), and the epidermis and dermis (E–D). Refraction at these interfaces gives

$$n \sin\theta = n_{sc} \sin\theta_{sc} = n_e \sin\theta_e = n_d \sin\theta_d \quad \text{(C.3)}$$

in which n, n_{sc}, n_e, and n_d are the refractive indices of the immersion medium, stratum corneum, epidermis and dermis, θ is the angle of incidence, and θ_{sc}, θ_e and θ_d are the angles of refraction at the I–SC, SC–E, and E–D interfaces, respectively. (As NA = n sinθ, it remains the same in all media.) When equation (C.1) is applied at each interface, we get the actual depth of the objective lens focal plane relative to the apparent (nominal) depth:

$$z_{sc} = \frac{\tan\theta}{\tan\theta_{sc}} \; z_{sc} \quad \text{(C.4)}$$

at the I–SC interface, where z_{obj} is the apparent depth below the I–SC interface (i.e., the depth through which the objective lens has been translated);

$$z_e = \frac{\tan\theta_{sc}}{\tan\theta_e} \; (z_{sc} - t_{sc}) \quad \text{(C.5)}$$

at the SC–E interface, where t_{sc} is the thickness of the stratum corneum;

$$z_d = \frac{\tan\theta_e}{\tan\theta_d} \; (z_e - t_e) \quad \text{(C.6)}$$

at the E–D interface, with t_e being the thickness of the epidermis.

For the 30 ×/0.9 NA objective lens, the angle of incidence θ is 42.6° (as NA = n sinθ, and n = 1.33 for water). The refractive indices of the stratum corneum (n_{sc} = 1.51), epidermis (n_e = 1.34), and dermis (n_d = 1.40) are known from recent measurements by optical coherence tomography (Tearney *et al*, 1995). Thus, we calculate from equation (C.3) the angles of refraction: θ_{sc} = 36.6°, θ_e = 42.1°, and θ_d = 40.0°. We have measured the thickness of the stratum corneum (t_{sc} = 20 μm) and epidermis (t_e = 100 μm). For the objective lens translation (i.e., apparent depth) of z_{obj} = 350 μm, equations (C.4), (C.5), and (C.6) give z_{sc} = 433 μm, z_e = 340 μm, and z_d = 258 μm. Thus, from **Fig C2**, we estimate the actual maximum depth of imaging: $t_{sc} + t_e + z_d$ = 378 μm.

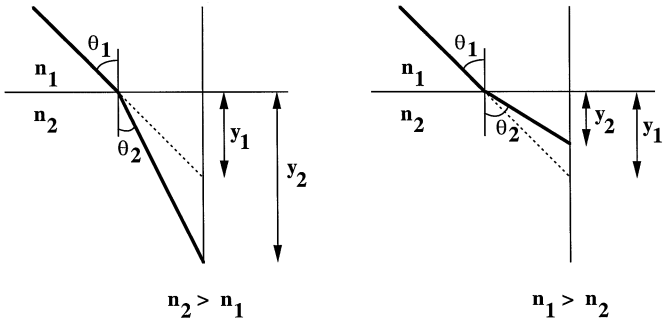

Figure C1. Refraction at the interface between two media causes a light ray to bend. Equation (C.1) defines the actual depth y_2 of the refracted ray relative to the apparent or nominal depth y_1 (in the absence of refraction). The refractive indices of the two media are n_1 and n_2, and the angles of incidence and refraction are θ_1 and θ_2.

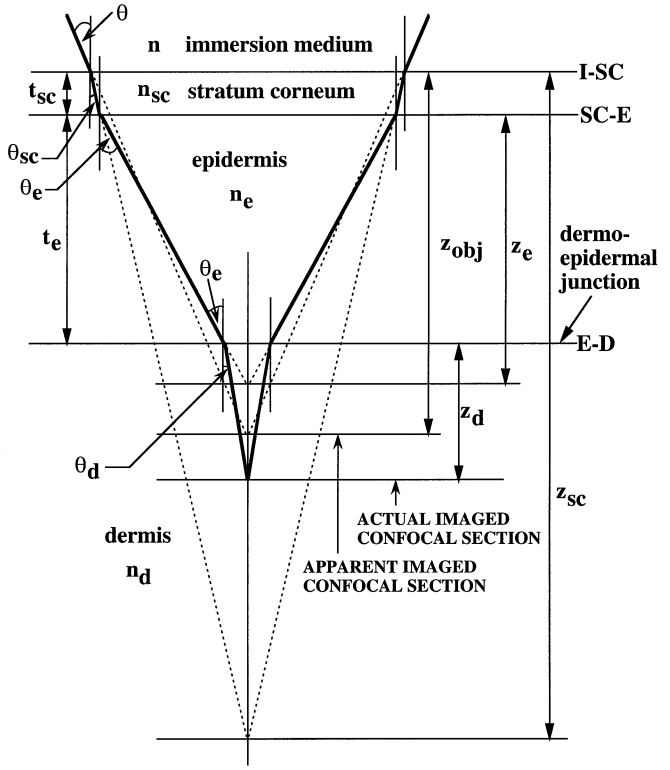

Figure C2. The immersion medium (water) and the three layers (stratum corneum, epidermis, dermis) of the skin are modeled as plane parallel layers with uniform refractive indices. The measured refractive indices are n = 1.33 (water), n_{sc} = 1.51 (stratum corneum), n_e = 1.34 (epidermis), and n_d = 1.40 (dermis). The measured thickness are t_{sc} = 20 μm (stratum corneum) and t_e = 100 μm (epidermis). Refraction occurs at the interfaces between the immersion medium and stratum corneum (I–SC), the stratum corneum and epidermis (SC–E), and the epidermis and dermis (E–D). The angle of incidence is θ, and the angles of refraction are θ_{sc}, θ_e, and θ_d. The depth through which the objective lens has been translated (i.e., apparent depth below the I–SC interface) is z_{obj}, for which the actual depth of the imaged confocal section is ($t_{sc} + t_e + z_d$), calculated from equation. (C4) to (C.6).